



Piezoelectrical properties for SnO₂ thin films prepared by spray pyrolysis method

Ali Jasim Mohammed Al-Jabiry, Muhaj Talib Abdullah, Marwa Abdul Muhsien Hassan

Department of physic, College of Science, Al-Mustansiriyah University, Baghdad, Iraq

Received 13 February 2013; Revised 19 April 2013; Accepted 3 June 2013

Abstract

Transparent conducting tin oxide (SnO₂) thin film has been deposited on glass substrate by spray pyrolysis technique. The spray pyrolysis technique using material tin chloride solution (SnCl₄.5H₂O) starts at different substrate temperature. The XRD result shows a regular, smooth morphology. The deposited film was found to be polycrystalline. The average grain size of SnO₂ was found to be (12.6-20.2) nm as calculated by XRD using Debye Scherrer Formula. The optical absorption, transmittance and optical band gap have been measured. It was found that the average transmittance of the film is around 79% at substrate temperature 500°C within wavelength range (300-800)nm. SnO₂ films have indirect piezoelectric phenomena where the particle was polarized when we applied an electrical current and its mechanical stress, hence the electrical force transformed into mechanical stress.

Keywords: SnO₂; structure properties; piezoelectric properties; resonance frequency; Damping Coefficient.

PACS: 78.40.Fy, 77.65.Dq, 78.66.Jg.

1. Introduction

Transparent conducting oxide coatings are important element in a large number of applications, due to the unique combination of high electrical conductivity with good optical transmission in the visible range [1]. SnO₂ belongs to the important family of oxide materials that combines low electrical resistance with high optical transparency in the visible range of the electromagnetic spectrum [2]. Typical fields of applications for such coatings are, *e.g.*, the use as electrodes in displays, solar cells and heating elements or in the provision of electromagnetic shielding maintaining transparency, defrosting windows, low emissivity windows or antistatic properties [1–3]. SnO₂ is chemically inert, mechanically hard and can resist high temperature [4]. There are many techniques, including sputtering, evaporation and chemical vapor or spray deposition, by which the SnO₂ films may be deposited on glass substrates. In this study, tin oxide thin films were prepared by the spray pyrolysis technique [5]. Spray pyrolysis method has the advantages of low cost, ease of operation and the possibility to coat large surfaces in mass production. The influence of experimental parameters such as concentration of precursor, deposition temperature,

deposition time, doping concentration and growth rate on the morphology, conductivity and optical transmittance of SnO₂ films have been investigated in order to obtain thin uniform films of necessary quality for optoelectronic devices [6-8]. Piezoelectric sensors have broad frequency response, high sensitivity, high signal-to-noise ratios, better environment adaptability, simple structure, reliable operation, small volume, light weight etc. However, their precision of measuring force is usually inferior to that of the strain sensors and they are worse than capacity sensors on displacement precision. In addition to the interference of secondary instruments, the main reason is that only first piezoelectric effect is applied in traditional piezoelectric sensors, but secondary and multiple piezoelectric effect that exists in nature are neglected. In that case, the application on super-precision measurement for piezoelectric sensors is limited. The primary research goal of multiple piezoelectric effects is to resolve the bottleneck of low testing precision of first piezoelectric effect and key problems of high precision, small force and small displacement [9].

Piezoelectricity is the charge which accumulates in certain solid materials (notably crystals, certain ceramics and biological matter such as bone, DNA and various proteins) [10], in response to applied mechanical stress. The word piezoelectricity means electricity resulting from pressure. It is derived from the Greek piezo or piezin, which means to squeeze or press and electric which stand for amber, an ancient source of electric charge [11]. Piezoelectricity is the direct result of the piezoelectric effect. The piezoelectric effect is understood as the linear electromechanical interaction between the mechanical and the electrical state in crystalline materials with no inversion symmetry [12]. The piezoelectric effect is a reversible process in that materials exhibiting the direct piezoelectric effect (the internal generation of electrical charge resulting from an applied mechanical force) also exhibit the reverse piezoelectric effect (the internal generation of a mechanical force resulting from an applied electrical field) [13]. Fig. 1 illustrates the piezoelectric effect. Fig. 1 shows the piezoelectric material without a stress or charge. If the material is compressed, then a voltage of the same polarity as the poling voltage will appear between the electrodes (b). If stretched, a voltage of opposite polarity will appear (c). Conversely, if a voltage is applied the material will deform. A voltage with the opposite polarity as the poling voltage will cause the material to expand (d) and a voltage with the same polarity will cause the material to compress (e). If an AC signal is applied then the material will vibrate at the same frequency as the signal (f) [14].

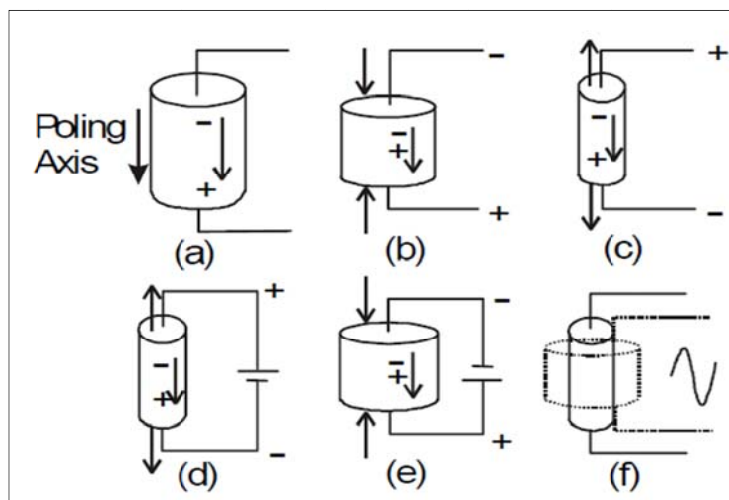


Fig. 1: Piezoelectric Phenomena.

Piezoelectric behavior in general can be manifested in two ways ‘direct’ piezoelectric effect and ‘converse’ piezoelectric effect. Direct piezoelectric effect occurs when a piezoelectric material becomes electrically charged when subjected to a mechanical stress. These devices can be used to detect strain, movement, force, pressure or vibration by developing appropriate electrical responses, as in the case of force and acoustic or ultrasonic sensors. Converse piezoelectric effect occurs when the piezoelectric material becomes strained when placed in an electric field. This property can be used to generate strain, movement, force, pressure or vibration through the application of suitable electric field. Although the magnitudes of piezoelectric voltages, movements, or forces are small, and often require amplification piezoelectric materials have been adapted to an impressive range of applications. The piezoelectric effect is used in sensing applications, such as in force or displacement sensors. The inverse piezoelectric effect is used in actuation applications, such as in motors and devices that precisely control positioning and in generating sonic and ultrasonic signals [14].

A. The Effect of Stress Direction on the Piezoelectricity

Fig. 2 shows the tetragonal unit cell without and with external stress [15]. Such unit cell is called non-centrosymmetric, when unstressed as in Fig. 2 (a). The center of negative charge masses coincide with the center of the positive charges. However when the unit cell is stressed as shown in Fig. 2 (b), the positive charge at (A) and the negative charge at (B) both become displaced inwards to (A') and (B') these shifts produce a net polarization (p) in the unit cell. In this case, the polarization appears in the same direction as the applied stress.

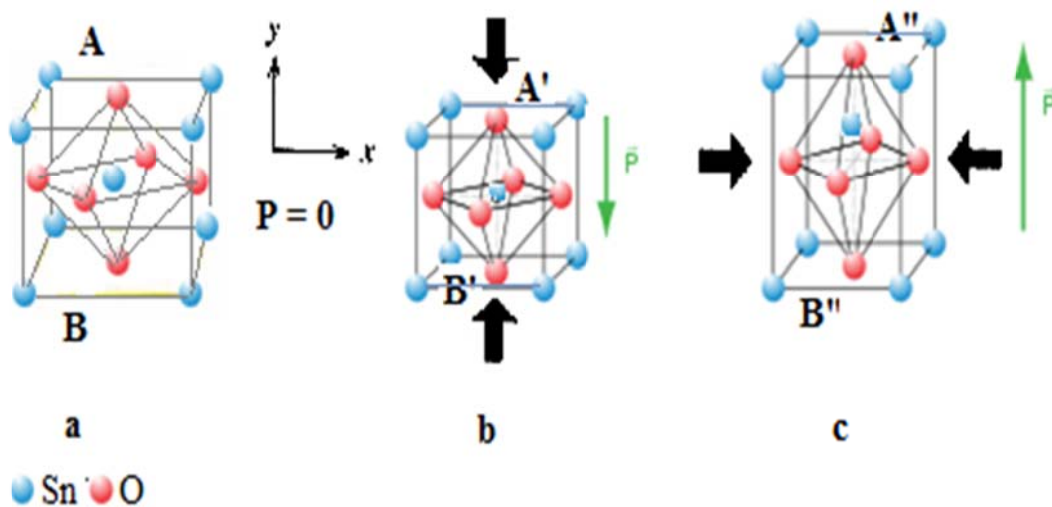


Fig. 2: The strain of a tetragonal unit cell.

The tetragonal unit cell in Fig. 2 (c) is with no induced dipole moment along the same direction of the applied stress because there is no net displacement of the center of mass and the atoms are displaced towards (A'') and (B''). The applied stress along (x) direction induces a polarization along (y) direction, so in general “*an applied stress in one direction can give rise to induced polarization in other crystal directions*”.

B. The Piezoelectric Effect Works

The piezoelectric effect occurs when the charge balance within the crystal lattice of a material is disturbed. When there is no applied stress on the material, the positive and negative charges are evenly distributed so there is no potential difference. When the lattice is changed slightly, the charge imbalance creates a potential difference, often as high as several thousand volts. However, the current is extremely small and only causes a small electric shock. The converse piezoelectric effect occurs when the electrostatic field created by an electrical current causes the atoms in the material to move slightly, where the material is heated under the application of a strong electric field. The heat allows the molecules to move more freely and the electric field forces all of the dipoles in the crystal to line up and face in nearly the same direction as shown in Fig. 3 [16].

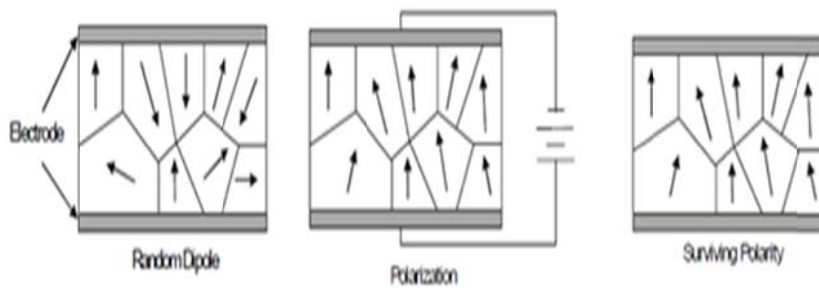


Fig. 3: The polarization of material to generate piezoelectric effect.

C. Piezoelectric Characteristics

Certain crystals possess a permanent electrical dipole because their centers of positive and negative charges are not at the centers of the unit cells. These unit cells are polarized [16]. Many materials change their dimensions in an electric field because the negative charges are pulled towards the positive electrode, and the positive charges are pulled towards the negative electrode as shown in Fig. 4 [15]. The pulling of the charges will increase the dipole length (d), this also increases the dipole moment (Q_d) and the polarization (p), since the latter is the total of the dipole moment ($\sum Q_d$) per unit volume (V) [17]:

$$P = \sum Q_d / V \tag{1}$$

This sequence of effects provides the means of changing mechanical energy into electrical energy and vice versa.

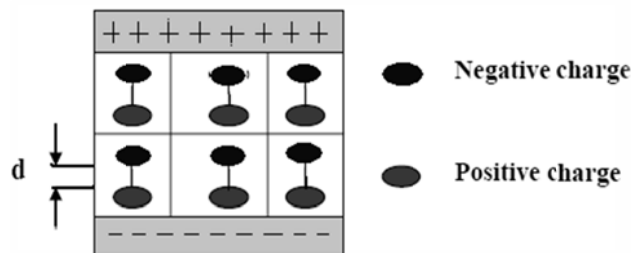


Fig. 4: The charges pulled toward the opposite electrodes.

D. Piezoelectric Coefficients

Because a piezoelectric is anisotropic, physical constants relate to both the direction of the applied mechanical or electric force and the directions perpendicular to the applied force. Consequently, each constant generally has two subscripts that indicate the directions of the two related quantities, such as stress and strain for elasticity. The direction of positive polarization usually is made to coincide with the Z-axis of a rectangular system of X, Y, and Z axis Fig. 5. Direction X, Y, or Z is represented by the subscript 1, 2 or 3 respectively and shear about one of these axis is represented by the subscript 4, 5 or 6 respectively [15].

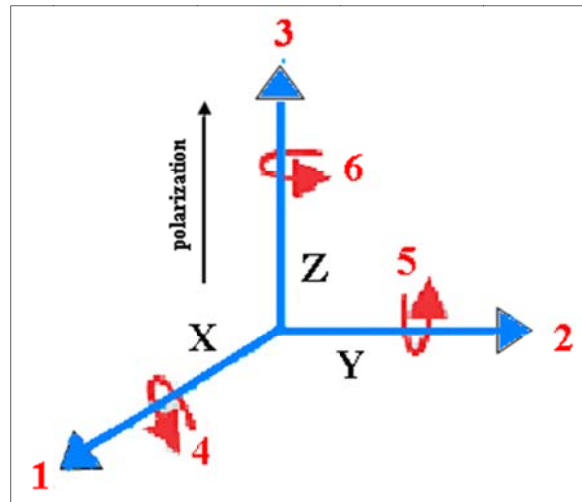


Fig. 5: Direction of force affecting a piezoelectric element.

i - Piezoelectric Charge Constant (d_{ij})

The *piezoelectric charge constant*, d_{ij} is the polarization generated per unit of mechanical stress (T) applied to a piezoelectric material or alternatively is the mechanical strain (S) experienced by a piezoelectric material per unit of electric field applied. The first subscript (i) to (d_{ij}) indicates the direction of polarization generated in the material when the electric field, E, is zero or, alternatively, is the direction of the applied field strength. The second subscript (j) is the direction of the applied stress or the induced strain, respectively. Because the strain induced in a piezoelectric material by an applied electric field is the product of the value for the electric field and the value for d, d is an important indicator of a material's suitability for strain-dependent (actuator) applications [15]. d_{33} induced polarization in direction 3 (parallel to direction of polarized) per unit stress applied in direction 3 or induced strain in direction 3 per unit electric field applied in this direction 3 [14].

ii - Piezoelectric Voltage Constant (g_{ij})

The piezoelectric voltage constant (g_{ij}) is the electric field generated by a piezoelectric material per unit of mechanical stress applied or alternatively, is the mechanical strain experienced by a piezoelectric material per unit of electric displacement applied. The first subscript (i) to (g_{ij}) indicates the direction of the electric field generated in the material, or the direction of the applied electric displacement. The second subscript (j) is the direction of the applied stress or the induced strain, respectively. Because the strength of

the induced electric field produced by a piezoelectric material in response to an applied physical stress is the product of the value for the applied stress and the value for g , g is important for assessing a material's suitability for sensing (sensor) applications. g_{31} induced electric field in direction 3 per unit stress applied in direction 1 or induced strain in direction 1 per unit electric displacement applied in direction 3 [14]. Piezoelectric transducers are widely used to generate ultrasonic waves in solids and also to detect such mechanical waves as shown in Fig. 6 where the transducer on left is excited from an AC source and vibrates mechanically, these vibrations are coupled to the solid and generate elastic wave, when the waves reach the other end, they mechanically vibrate the transducer on the right, which convert the vibration to an electrical signal [18].

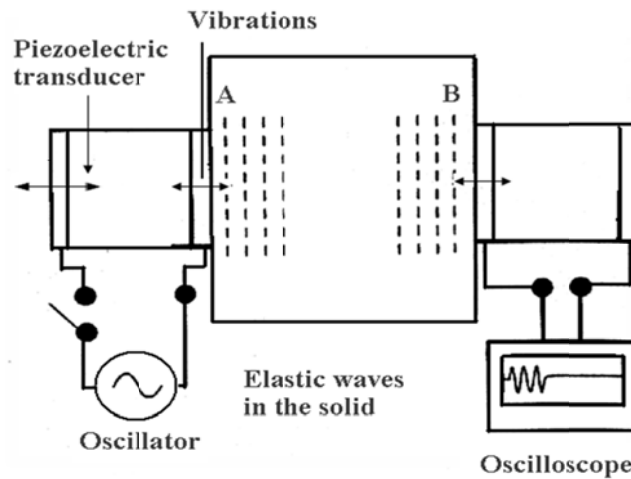


Fig. 6: The mechanism of piezoelectric application.

E. Resonance Frequency (f_0)

When an unrestrained piezoelectric element is exposed to a high frequency alternating electric field, it changes dimensions cyclically at the cycling frequency of the field. The frequency at which the element vibrates most readily and most efficiently converts the electrical energy input into mechanical energy is the resonance frequency, when impedance minimum, the planar or radial resonance frequency, coincides with the series resonance frequency, f_s . At higher frequencies resonance, another impedance minimum, the axial resonance frequency, is encountered [19]. This frequency is characterized by the output amplitude as shown in Fig. 7 [20].

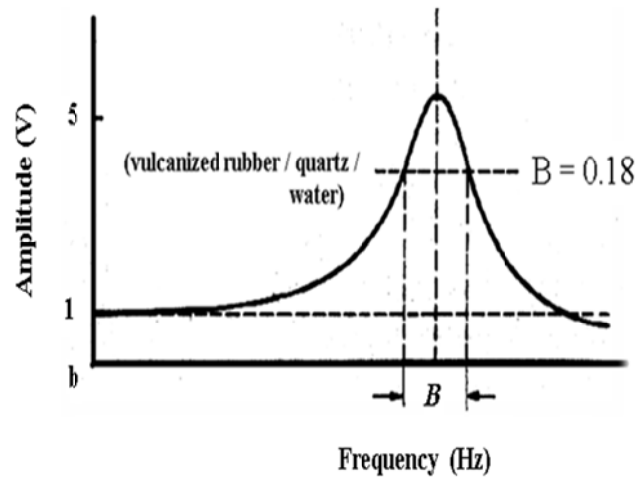


Fig. 7: Resonance curve of forced oscillation.

Up to the resonance frequency (f_o) it increases to a maximum, where the value depends on the damping coefficient.

F. Characteristic Frequency (f_e)

The characteristic (fundamental) frequency (f_e) will be considered as the oscillation of the particles on both surfaces of the block material of the thin film, when the two electrodes are contacted the particle swings outwards and inwards [20], while the central plate remains constantly at rest. Hence a standing wave will be produced and the characteristic frequency is related to the plate thickness as in relation:

$$t = \lambda/2 = V_s/2f_e \quad (2)$$

where

t = The plate thickness,

V_s = The velocity of sound.

G. Damping Coefficient (δ)

Damping is an important characteristic of structural mechanical vibrating systems. A reasonably accurate input damping data is needed to design the system under different vibratory loadings. Inaccurate estimation of damping may lead to failure of systems during service. In general, damping can be classified into two categories i.e., material damping and system damping. Material damping is defined as “the inherent property of any material to dissipate energy in a volume of macro continuous media”. System damping relates to “energy dissipation in total structure”. It includes energy dissipation effects of joints, fasteners and interfaces in addition to energy dissipation due to material. Mechanical vibration damping can be defined as the ratio of energy dissipated to maximum strain energy per cycle of vibration [21]. Damping is a material property, which is very important to vibration control in engineering. The numerical results of vibration and acoustical analysis are very sensitive to this parameter. For the mechanical damping treatment of structure is necessary to consider three parameters: damping; mass and stiffness. These three parameters are needed to design and optimize piezoelectric transducers by using numerical modeling since all of them have some effect in piezoelectric transducer dynamic response.

In addition, most part of systems that dissipate energy by vibration is non-linear. Therefore, it is necessary to develop models of ideal damping with suitable approximation. The several types of damping are [22]:

- 1- Viscous damping, due to energy dissipation;
- 2- Structural damping, due to the material properties;
- 3- Friction damping, due to mechanical sliding between surfaces.

The damping coefficient (δ) is the factor that the amplitude will be decreased from one oscillation to the next oscillation according to it as in the Fig. 8 [23] and the damped amplitude is given by the relation [24]:

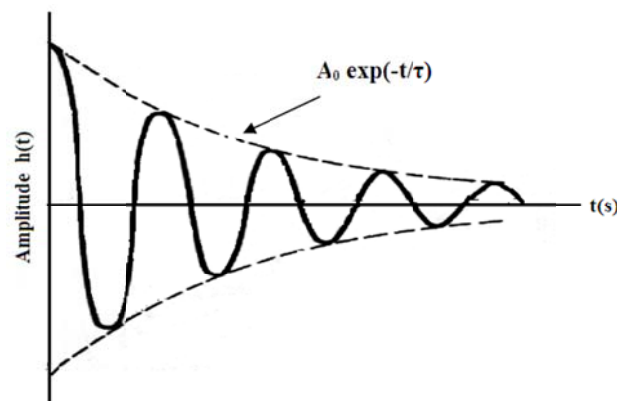


Fig. 8: Decay of oscillation with damping coefficient δ .

$$h(t) = A_o \exp(-t/\tau) \sin(\omega t) \quad (3)$$

where:

- A_o = The amplitude at resonance
- t = $1/f$, (f) is the frequency
- ω = $2\pi \tau$
- τ = The resonance time

H. Quality Factor (Q)

To achieve ultra-high resonator sensitivity, high quality factor (Q-factor) is most desirable in resonator design and fabrication [24]. Under atmospheric pressure, air damping is the predominant mechanism for energy dissipation [25]. Air damping becomes less effective if pressure goes down and then it is easier to identify the effects of other energy dissipation mechanisms [26]. The Q can be defined as the ratio of the amplitude at resonance frequency to the static thickness:

$$Q = \Delta X_{fo} / \Delta X_{stat} \quad (4)$$

Also it is connected to the damping coefficient (δ) as in relation:

$$Q = \pi / \ln \delta \quad (5)$$

The higher order modes achieve higher frequencies and the increase of resonance frequency will decrease the Q-factor [27].

I. Bandwidth (B)

The bandwidth (B) is linked with resonance frequency, which represents 70% from the maximum value of the resonance frequency, normally it is calculated from the resonance curve, then the characteristic frequency can be calculated by using the relation [20]:

$$B = f_e/Q \quad (6)$$

where:

f_e = The characteristic frequency.

2. Experimental Details

2.1 Solution Preparation

SnO_2 thin film has been successfully deposited by chemical spray pyrolysis method. The film is deposited using 0.4M tin chloride ($\text{SnCl}_4 \cdot 5\text{H}_2\text{O}$) dissolved in distilled water, ($\text{SnCl}_4 \cdot 5\text{H}_2\text{O}$) is a solid material which has a white color and its molecular weight (350.85 ml/mol). The sprayed solution was deposited on the glass substrate that was carefully cleaned with dilute HCl and finally cleaned with acetone. The deposition method involves the decomposition of an aqueous solution of tin chloride. The spray solution of 0.4M was sprayed onto different heated substrates temperatures (400, 450, 500 and 550) $^\circ\text{C}$. The compressed air was used as a carrier gas and it was fed with the solution into a spray nozzle at a pre-adjusted constant atomization pressure. The nozzle to substrate distance was (26 ± 2) cm and the spraying period was (3 sec/min) and the spray rate was maintained 0.5ml/min. The chemical reaction of the growth is shown in Fig. 9(a).

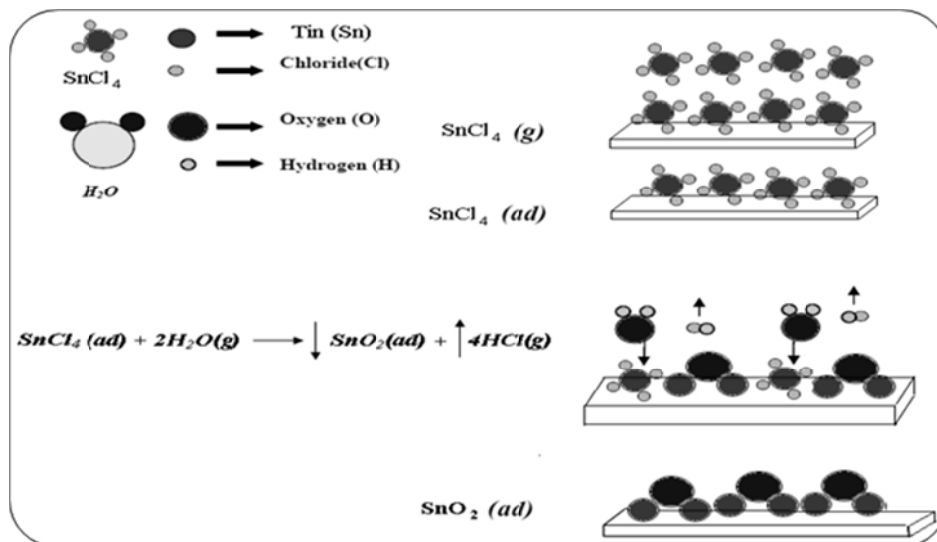


Fig. 9(a): The chemical reaction of SnO_2 growth on the substrate.

The schematic diagram of the experimental work starting from material up to films characterization is displayed in Fig. 9(b).

0.4 Molarity (M) $\text{SnCl}_4 \cdot 5\text{H}_2\text{O}$

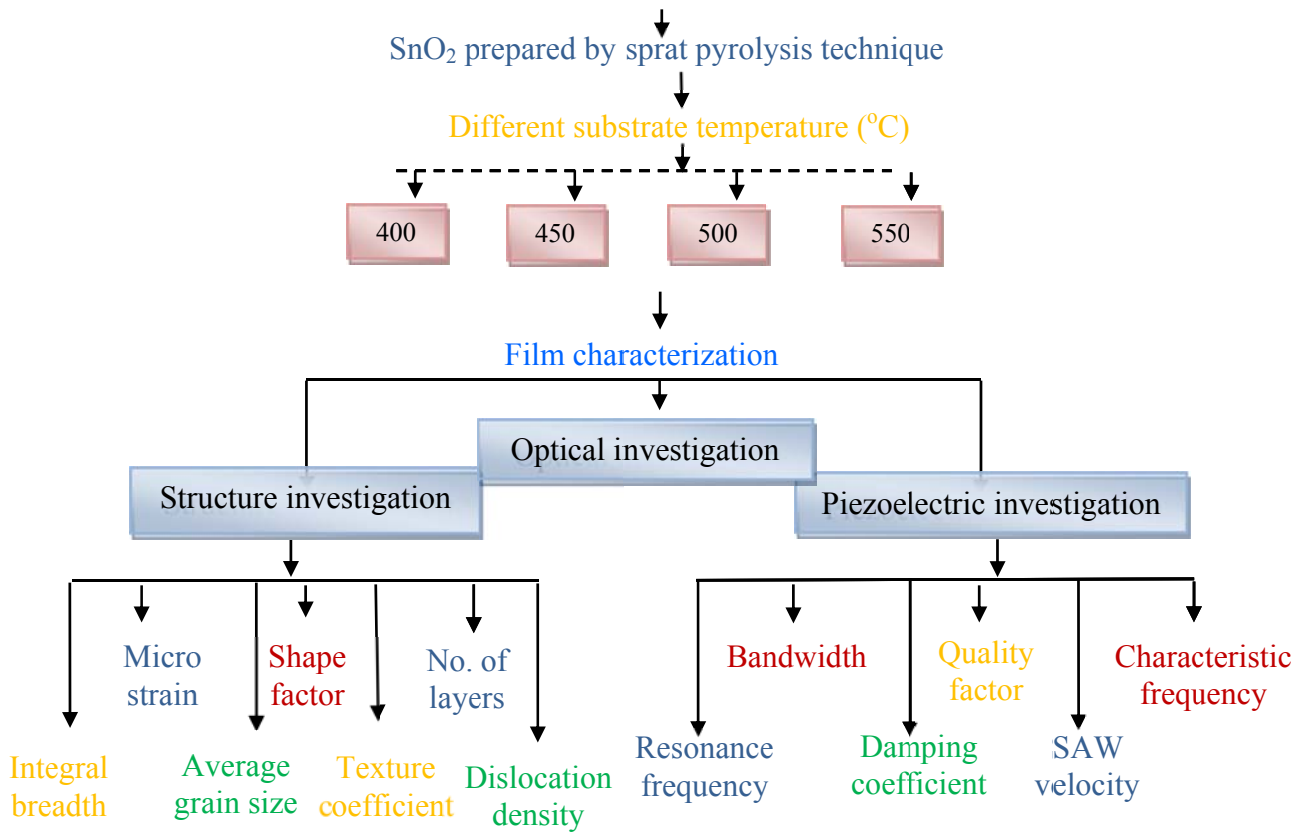


Fig. 9(b): The schematic diagram of the experimental work.

2.2 Electrodes Deposition

Aluminum sheets were used as a mask. These masks are placed on films to deposit the aluminum on the surface of (SnO₂) films by using thermal evaporation equipment type (Edward), the electrodes deposited by using aluminum wire placed in (Tangiesten W) boat material under pressure (10⁻⁵ Torr), then the aluminum electrodes deposited on the thin films with diameters (1.5*1.5)cm² with thickness approximately (150)nm, through a mask giving sensitive area (0.5*0.5)cm² as illustrated prepared as in Fig. 10.

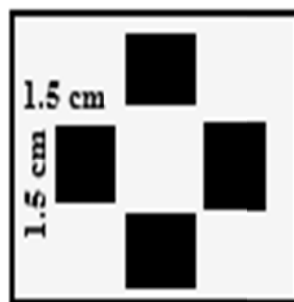


Fig.10: The mast pattern which used in piezoelectric measurements.

2.3 Characterization of SnO₂ Thin Film

The Film Topography of the SnO₂ thin films prepared under various preparation conditions were investigated with an optical microscope (500X magnification power type

Nikon ECLIPSE ME600). A digital Camera (DXM1200F) connected to a computer to analyze the surface image of the prepared films. The structure analysis and lattice parameters of films were carried out by analyzing the x-ray diffraction patterns obtained via an instrument type (Shimad Zu 6000). The piezoelectric sensing of SnO₂ film samples was measured using hand setting as shown in figure 11-a. This setting used a standard piezo crystal (Model number: 3B12+9.0EAWC, Type: Piezoelectric Ceramics, Material: Piezoceramics, Metal type: Brass, Electrode form: (Thin) Diode, Connection terminal: Soldier wire or not, Parameter value: (D = 12mm, T = 0.15mm and f = 9 kHz) located tightly on the copper foil as a diaphragm shown in figure (11-b). The pressure (mechanical) signal was produced on the diaphragm (interface) using a function generator Philips supplied an electrical signal of frequency in the range (10–10000)KHz.

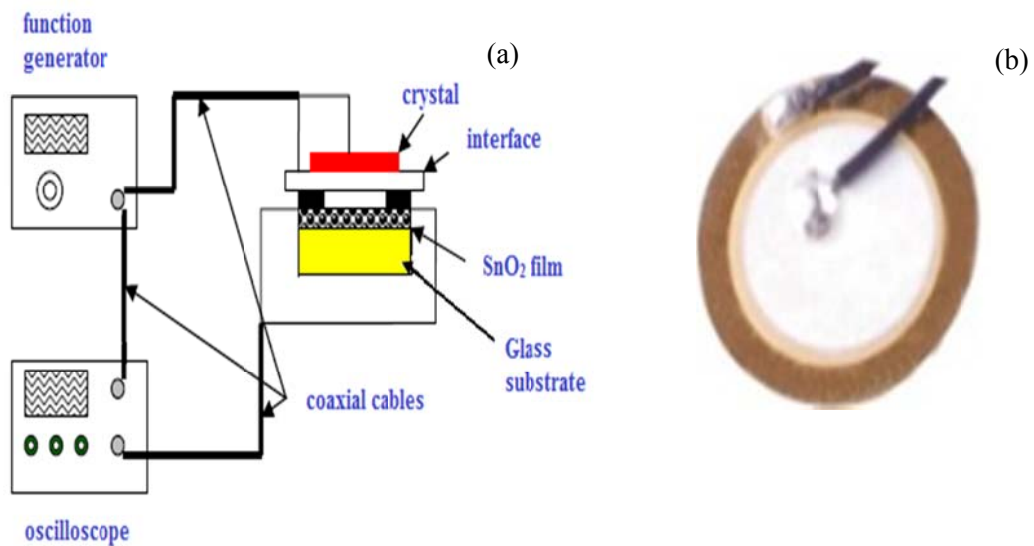


Fig. 11(a): The setting of piezoelectric sensing measurement of SnO₂ film. (b) Image of piezo-crystal used in this work.

3. Result and Discussion

3.1 Structural Analysis of SnO₂ Film

3.1.1 Surface Morphology

We have studied the surface morphology of the produced TCO films. The following figures show the optical micrograph of SnO₂ thin films, those prepared at various growth conditions. These micrographs reveal that the film morphology can be easily recognized through the film homogeneity and color. Figure 12, gives the optical micrographs of the (0.4)M films morality deposited on glass substrate at (400, 450, 500, 550)^oC. The color of films tends to be white, which reflects the metallic nature of SnO₂, which typically has white color as well as the high transmission of the obtained film. It can clearly be noticed that the film color is the same as the physical color of the SnO₂ thin film.

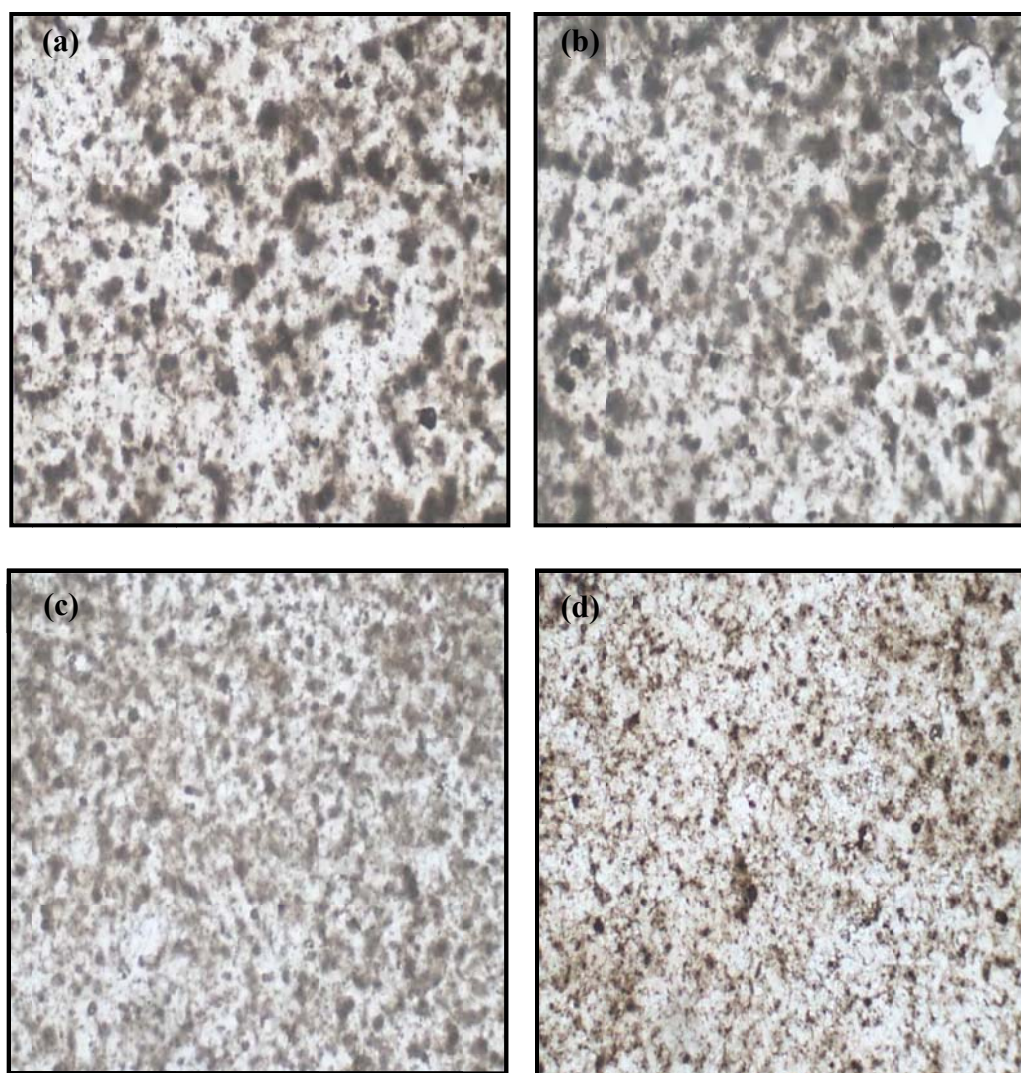


Fig. 12: Surface morphology of SnO₂ prepared with 0.4 M at different substrate temperature: (a) 400°C, (b) 450°C, (c) 500°C and (d) 550°C.

3.1.2 XRD pattern

It is known that tin dioxide SnO₂ has a tetragonal rutile crystalline structure (known in its mineral form as cassiterite) [28]. The unit cell consists of two metal atoms and four oxygen atoms. Each metal atom is situated amidst six oxygen atoms which approximately form the corners of a regular octahedron. Oxygen atoms are surrounded by three tin atoms which approximate the corners of an equilateral triangle. Structural analysis of the deposited SnO₂ film was carried out by using CuK α radiation, source having wavelength 1.5406 Å. The X-ray diffraction pattern of the film is recorded. Fig. 13(a), (b), (c), and (d) shows the XRD patterns of SnO₂ deposited at different substrate temperature (400, 450, 500, and 550)°C respectively. It is observed the growth of the films enhancing when the temperature increase and the peaks become more sharply and this means the average grain size increase when the temperature increase, the results show that the preferred direction was oriented in (110) at 2θ equal (26.6098°) and there is another peaks observed in (101), (200), (211) and (220) direction at 2θ equal (33.8515°, 38.0519°, 51.91576° and 54.85798°) respectively, which are consistent with the standard values for bulk SnO₂ (JCPDS-041-1445) [29]. The result of XRD used to calculated the structure parameters which include: 1- FWHM

decreases with increases the temperature that means the broadening of the line reduce due to vibration of temperature excepted for 550°C. 2- Average grain size increase and the dislocation density decrease with increases temperature. 3- Micro strain caused compressing in the film structure as the minus sign indicated. Table 1 and 2 shows the result of structure parameters.

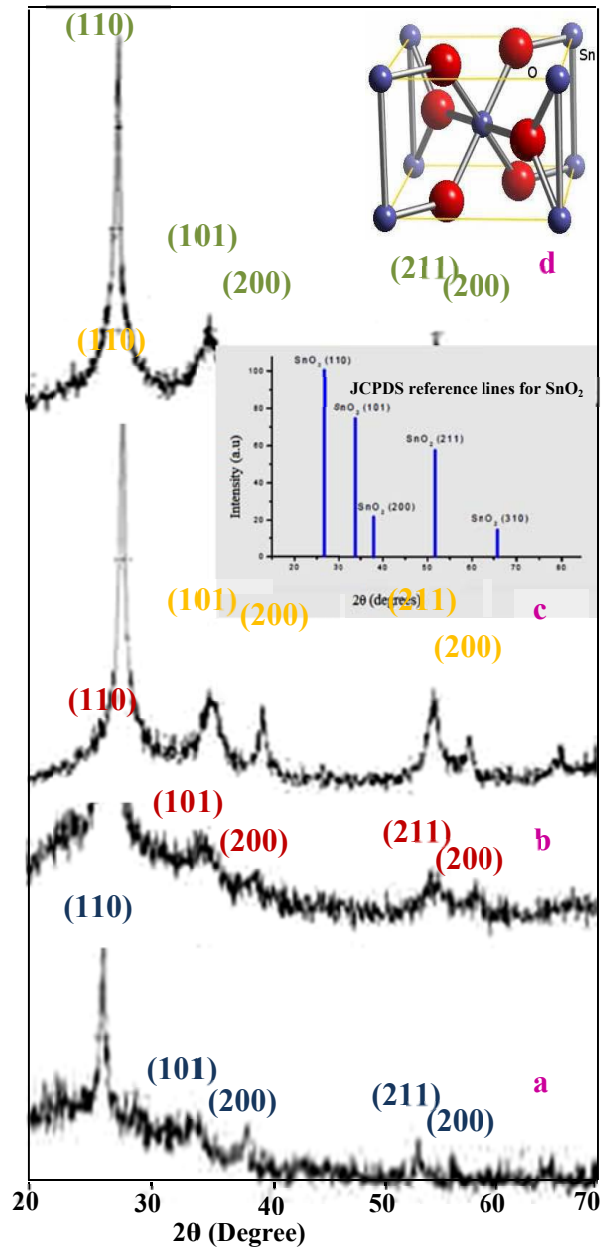


Figure 13: The XRD pattern of 0.4 M at different substrate temperature: (a)400°C, (b) 450°C, (c) 500°C and (d) 550°C.

i. Parameters Calculation

Normally XRD is used to calculate different parameters which could be used to clarify the studies of the deposited films.

A. Full Width at Half Maximum (FWHM) (Δ)

A full width at half maximum (FWHM) is an expression of the extent of a function, given by the difference between the two extreme values of the independent variable at which the dependent variable is equal to half of its maximum value. FWHM is applied to such phenomena as the duration of pulse waveforms and the spectral width of sources used for optical communications and the resolution of spectrometers. The term of "width" mean's "the broadened line profile" is also widely used in signal processing to define bandwidth as "width of frequency range where less than half the signal's power is attenuated" as show in figure 14, i.e. the power is at least half the maximum. When the considered function is the normal distribution of the form [30]:

$$f(x) = \frac{1}{\sigma\sqrt{2\pi}} \exp\left[-\frac{(x-x_0)^2}{2\sigma^2}\right] \quad (7)$$

Where (σ) is the standard deviation and (x₀) can be any value (the width of the function does not depend on translation).

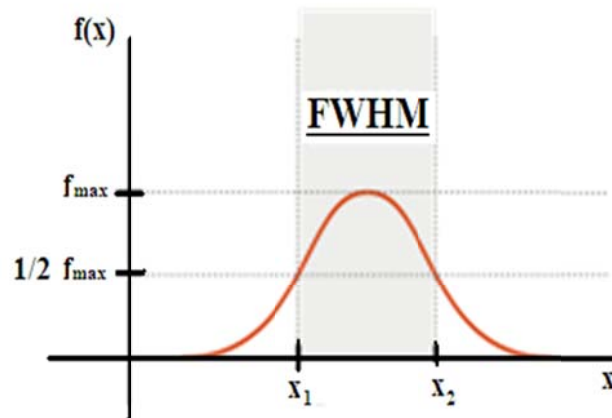


Fig. 14: Full Width at Half Maximum.

B. Broadening

The XRD peak is broadening due to small crystallite size and strain due to dislocations and stacking faults. The line profiles of the reflections of various planes during XRD are characteristic of the state of the material. There are many different types of broadening which appears in the output line, the first one is an instrument broadening caused by non ideal compound of the differactometer like slit width and wavelength width, dispersion, which must be correct to have the right crystallite size and the second is the structural imperfections of the specimen, also this branch is subdivided into size broadening (which is caused by the finite size of domains) and strain broadening (which is caused by

varying displacements of the atoms with respect to their reference-lattice positions) [31]. There are two basic technique of X-ray line profile analysis:

- i- Fourier space technique.
- ii- Real space technique like (a) integral breadth, (b) variance analysis, (c) peak fitting methods [32].

C. Integral Breadth (β)

Our study had been focused on the second type (real space technique), especially the integral breadth which is frequently characterized by means of one or two breadth measures FWHM and β which is given by [32]:

$$\beta = Area/I_{max} \quad (8)$$

where:

- β = Integral Breadth
- $Area$ = Area under the peak.
- I_{max} = Maximum intensity

D. Dislocations density (ρ)

Dislocation density is an important material properties which gives the length of the dislocations present per unit volume (m/m^3) [32]. The investigation methods of individual dislocations could be divided into four main groups [33]. The first method, known as the surface method is based on the formation of etch pits or hillocks at the site where a dislocation meets the surface. The second method is X-ray diffraction topography. This method introduces local differences at dislocations in the scattering of X-rays. The other method used by Hedges and Mitchell in 1985 is the decoration method [34]. The dislocation density investigated using the same method in β -Sn single crystals [35]. It is generally observed that dislocation density depends on crystal shape. Ojima and Hirokawa and Duzgun *et.al.* in 1967 showed that the dislocation density varies with the crystal shape [36].

The plot of the $\tan(\theta)$ on the x-axis and the $(\text{integral breadth})^2$ on the y-axis as shown in Fig. 15, we get the second order polynomial by fitting the result curved depending on the following equation to determined the value of U, V and W [32]:

$$(b)^2 = U \tan^2(\theta) + V \tan(\theta) + W \quad (9)$$

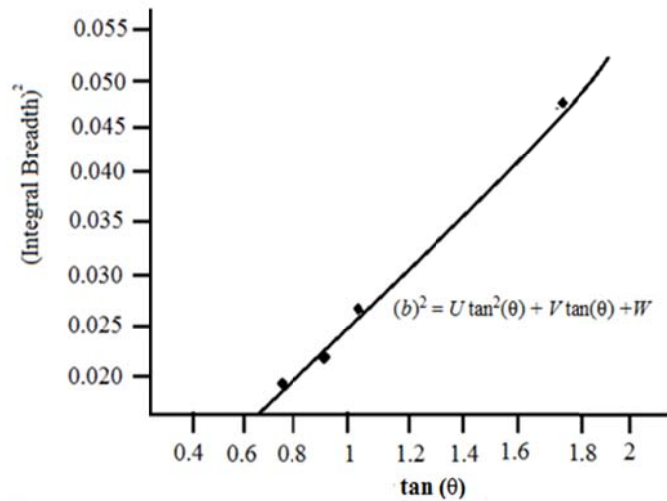


Fig. 15: The relation between integral breadth and tan (θ).

The plot of relation between $(\sin(\theta)/\lambda)^2$ and $(b\cos(\theta)/\lambda)^2$ result the linear relation as show in Fig. 16. From this figure the micro strain and coherent domain illustrated as the following [32]:

$$\begin{aligned} \text{Slope} &= 16 \varepsilon^2 \\ \text{Intercept} &= 1/D^2 \end{aligned}$$

Then the dislocation density (ρ_D) due to coherent small size is obtained from this relation [32]:

$$\rho_D = 3\eta / D^2 \tag{10}$$

where $\eta = 1$ and $1/D^2$ represent the intercept in the Fig. 16

The dislocation due to microstrain (ρ_ε) calculated from the relation [32]:

$$\rho_\varepsilon = 2k \varepsilon_L^2 / b^2 \tag{11}$$

where $k = 10$, ε_L : the strain.

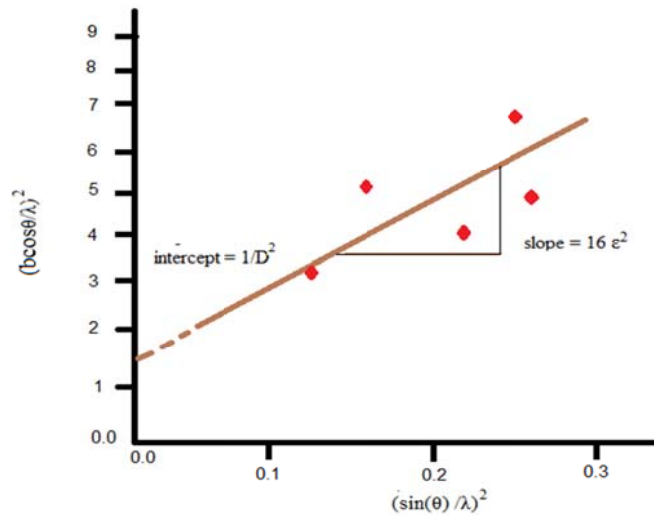


Fig. 16: The relation between $(b \cos\theta/\lambda)$ and $(\sin\theta/\lambda)$.

So the total dislocation density obtained from (ρ_D) and (ρ_ϵ) as following [37]:

$$\rho = (\rho_D \cdot \rho_\epsilon)^{1/2} \tag{12}$$

The X-ray line consists of contributions due to D and ϵ . Following relationship is used to separate the contributions from each of them for calculation of ρ [37]:

$$(\beta \cos(\theta)/\lambda)^2 = (1/D)^2 + (4\epsilon \sin(\theta)/\lambda)^2 \tag{13}$$

where β =instrumental corrected broadening (in radians), θ = Bragg's diffraction angle, D=coherent domain size (in Å), ϵ = micro strain and λ = wave length (in Å).

E. Determination of average grain size

The result line broadening of X-ray diffraction may refer to the defects in the crystal structure or to the asymmetry in strain between crystals, due to the small average grain size, so the reflection of X-ray from different parts of crystal will be in different angles which caused to increase the line broadening.

i. Scherer's average grain size formula

The average grain size can be calculated from Scherer [32]:

$$g = K \lambda / \Delta_{(2\theta)} \cos (\theta) \tag{14}$$

where:

λ = Wavelength of XRD

Δ = FWHM

Θ = Bragg's angle in degree

K = The correction coefficient variation according to the diffractometer and its magnitude about (0.9–1).

The other parameters are depending on the previous two parameters (FWHM and the integral breadth). These parameters are:

1. Shape Factor (Φ)

Depending on the results of X-ray diffraction and crystallography the shape factor is used to correlate the size of sub-micrometer particles or crystallites, in a solid to the broadening of a peak in a diffraction pattern, so the line profile resulting from the XRD patterns could be calculated from the relation [32]:

$$\Phi = \Delta / \beta \quad (15)$$

It is important to realize that the Scherer's formula provides a lower bound on the particle size. The reason for this is that a variety of factors can contribute to the width of a diffraction peak; besides particle size, the most important of these are usually inhomogeneous strain and instrumental effects. If all of these other contributions to the peak width were zero, then the peak width would be determined only by the particle size and the Scherer formula would apply. If the other contributions to the width are non-zero, then the particle size can be larger than that predicted by the Scherer formula, with the "extra" peak width coming from the other factors [32].

2. Texture Coefficient (T_C)

So to describe the crystallization, the texture coefficient, T_C (hkl) is calculated using the expression [33]:

$$T_C (hkl) = [I(hkl) / I_o(hkl)] / [N_r^{-1} \sum I(hkl) / I_o(hkl)] \quad (16)$$

where:

I = The relative intensity.

I_o = The ASTM relative standard intensity.

N_r = The number of reflections.

(hkl) = Miller indices.

The (T_C) depends on the molarity of the precursor solution; the high c-axis orientation at higher molarity is due to the combined effect of increase in Sn incorporation, increase in growth rate and re-orientation effect as shown in figure 17 [34].

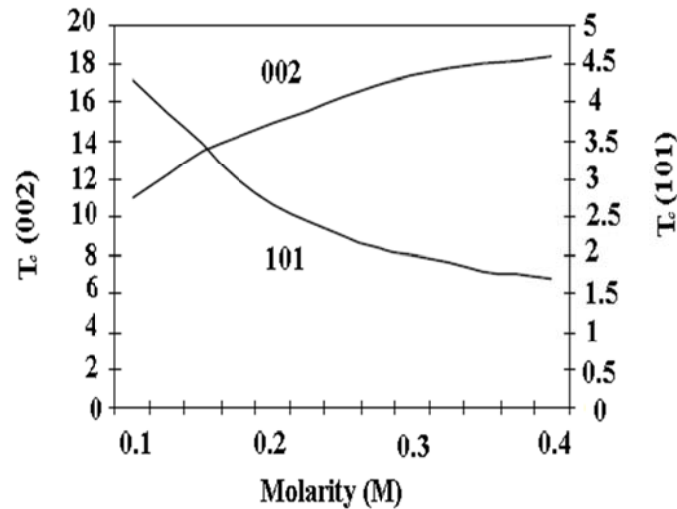


Fig. 17: Variation of $T_C(002)$ and $T_C(101)$ of ZnO: I thin films of different molarities.

3. Number of Layers (N_ℓ)

For the thin films the micro structural factor like film texture may be considered as the powerful means that control electrical properties of polycrystalline film materials [35]. Depends on the film thickness (t) the number of crystallite layer (N_ℓ) could be calculated using this relation [36]:

$$N_\ell = t_t/g \quad (17)$$

where:

- g = A mean crystallite size.
- t_t = The thickness of the film.

4. Micro Strain (ε)

The micro strains are caused during the growth of thin films, and will be raised from tensile or compression in the lattice to make a deviation in the lattice constants of the structure from the ASTM value. So the strain broadening is caused by varying displacements of the atoms with respect to their reference lattice position [38]. This strain can be calculated from the formula [39]:

$$\varepsilon = [\lambda / g \sin(\theta)] - [\beta / \tan(\theta)] \quad (18)$$

Table 1: The main planes observed with different substrate temperature and there specifications

Sample	Temperature	110			101			200		
		2 θ	I/I ₀	d(nm)	2 θ	I/I ₀	d(nm)	2 θ	I/I ₀	d(nm)
ASTM		26.611	100	0.333	34.195	75	0.262	37.949	21	0.233
0.4	400	26.5483	100	0.33548	34.0721	31	0.26925	38.052	31	0.2363
	450	26.6098	100	0.33472	33.9014	16	0.264210	38.015	15	0.2365
	500	26.5633	100	0.33529	34.172	17	0.262179	37.985	24	0.2366
	550	26.5483	100	0.33548	34.0721	31	0.262925	38.052	31	0.2363

Table 2: The Integral breadth–dislocation density data of investigated thin films

Molarity (M)	Temperature (°C)	Investigated line	Integral breadth (β) (deg.)	FWHM (deg.)	Shape factor (Φ)	Micro strain % (ϵ)	Average grain size (g) (nm)	Texture coeff. (T _c)	No. of layers (N _t)	Dislocation density (ρ) 10 ¹⁴ (cm/cm ³)
0.4	400	110	1.43	0.675	0.472	-6.065	12.636	1.852	23	5.375
	450	110	1.37	0.642	0.467	-5.794	13.328	2.206	21	1.413
	500	110	0.85	0.44	0.518	-3.601	19.384	1.923	19	0.0069
	550	110	1.01	0.421	0.417	-4.282	20.259	1.852	18	0.000354

Lattice Constants (a, c)

SnO₂ thin films show a tetragonal structure and Polycrystalline nature with orientation (110) direction perpendicular to the substrate comparing with (ASTM data card 46-1088). This plane is strongly dependent on the deposition conditions.

The lattice constants belong to the (110) plane of undoped SnO₂ films deposited under various temperature are given in Table 3. The lattice constants obtained are found to be good agreement with ASTM data card 46-1088 powder SnO₂ sample.

Table 3: Lattice constants as a function of molarity of undoped SnO₂

Samples	Temperature	a ₀ (nm)	c ₀ (nm)
0.4	400	4.735	3.188
	450	4.744	3.194
	500	4.733	3.186
	550	4.741	3.192
ASTM	-	4.750	3.198

3.2 Optical Properties

The transmittance spectra recorded for the films deposited on glass substrates in the wavelength range of (300-900)nm is shown in Fig. 18(a). An uncoated (blank) substrate has been used as the reference for obtaining the transmittance spectra. From this figure, we can observed that the transmittance increase by increasing substrate temperature except for 550°C where the transmittance value decrease comportsing with other temperature this may occurring because of the increasing in the thickness. Through the study of transmittance

spectrum for all thin films the transmittance of the films found to be very high at wavelengths in visible region and the best transmittance observed at 500°C within region (300-900)nm, where the transmittance value reach 80%. While the absorbance spectrum was submitted to the relation [40]:

$$A = \log_{10}(1/T) \tag{19}$$

Where: A: the absorption, T: the transmittance. The behavior of absorption curves were inversely to the behavior of the transmittance curves and because of the last were higher so the absorption smaller and the Fig. 18 obvious the behavior of transmittance and absorption, as a function of wave length at different substrate temperature.

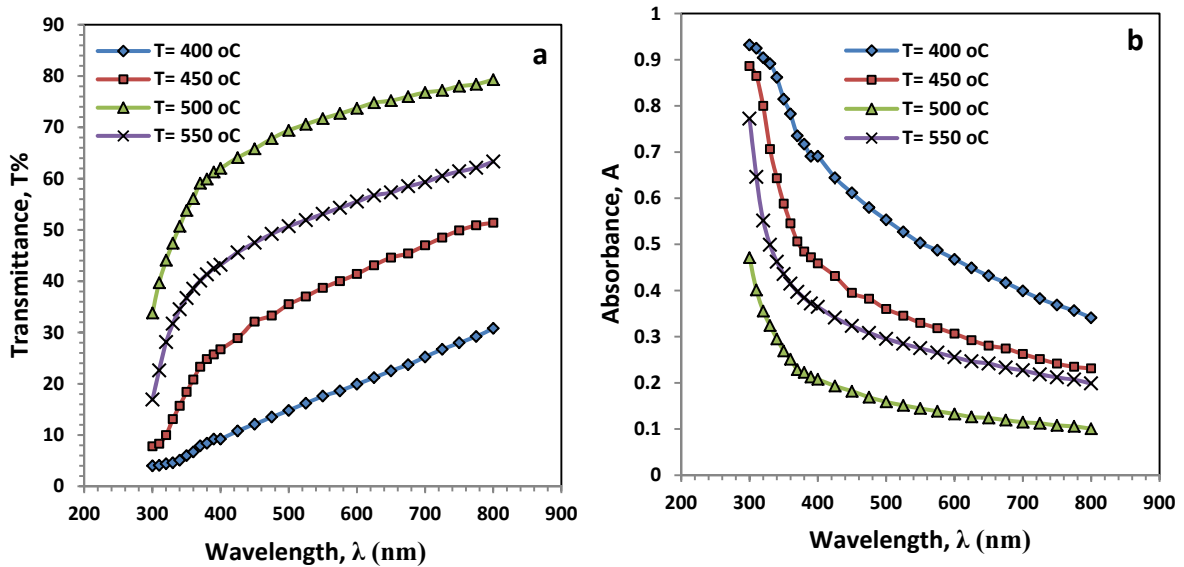


Fig. 18: Transmittance & Absorbance spectra of 150 nm SnO₂ films with wavelength at different substrate temperature (a)Transmittance, (b) Absorbance.

Fig. 19 shows the variation of $(\alpha hv)^2$ & (hv) for the determining the band gap E_g of SnO₂ film by extrapolation of curve. The incident photon energy is related to the direct band gap E_g by equation [40]:

$$(\alpha hv) \propto (hv - E_g)^{1/2} \tag{20}$$

The optical band gap was estimated in lower wave length region and it was found to be (2.8, 3.3, 3.6 and 3.7) eV.

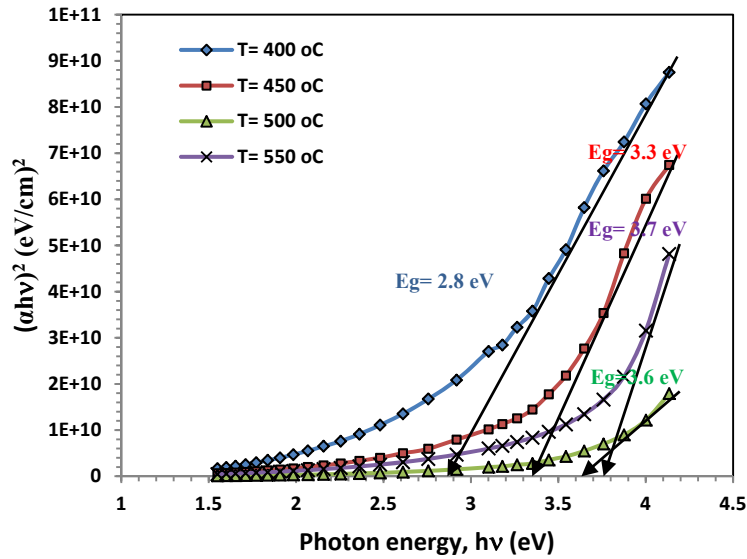


Fig. 19: Touge Plot of $(\alpha hv)^2$ with photon energy in SnO₂ thin film at different substrate temperature.

3.3 Piezoelectric properties

The piezoelectric properties of SnO₂ thin films can be observed in table 4 and mainly include:

1- The resonance frequency

The resonance frequency can be determined by measuring the output voltage as a function of frequency and the result show that the increasing in the temperature caused to shifting in the resonance frequency to higher ranges up to 10MHz as we shown in figure 20. This is meaning that the sensitive of the film enhance when the temperature increase this may be due to increasing in the homogeneity of the film and the arrangement of the grains.

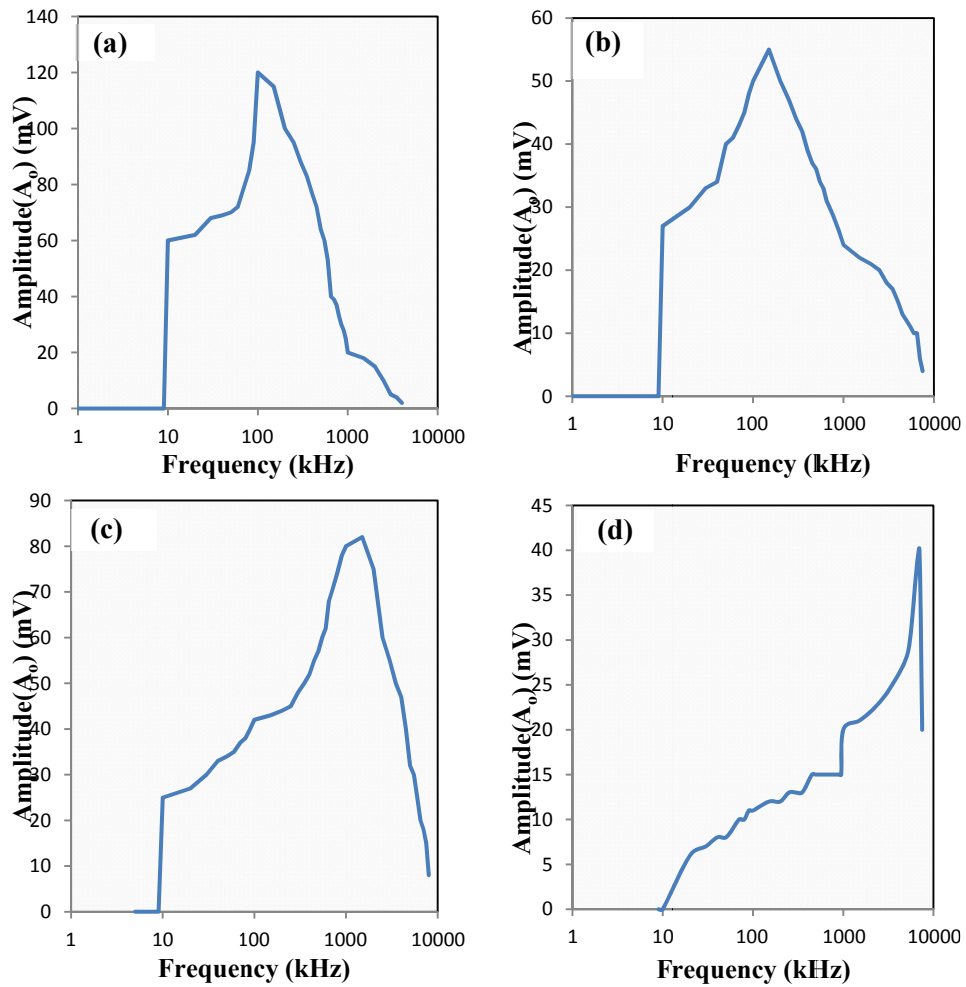
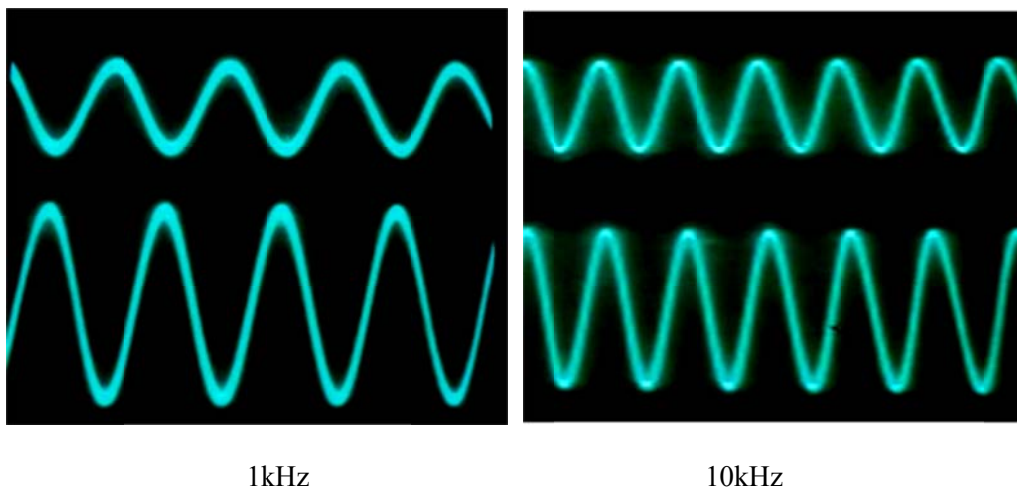


Fig. 20: The resonance frequency of 0.4 M at different substrate temperature: a-400, b-450, c-500 and d-550.

The shifting between the transmitted signal and that of SnO₂ for is shown in Fig. 21, it is clearly that the small shifting vanishes with increasing the source frequency and the temperature has no effect.



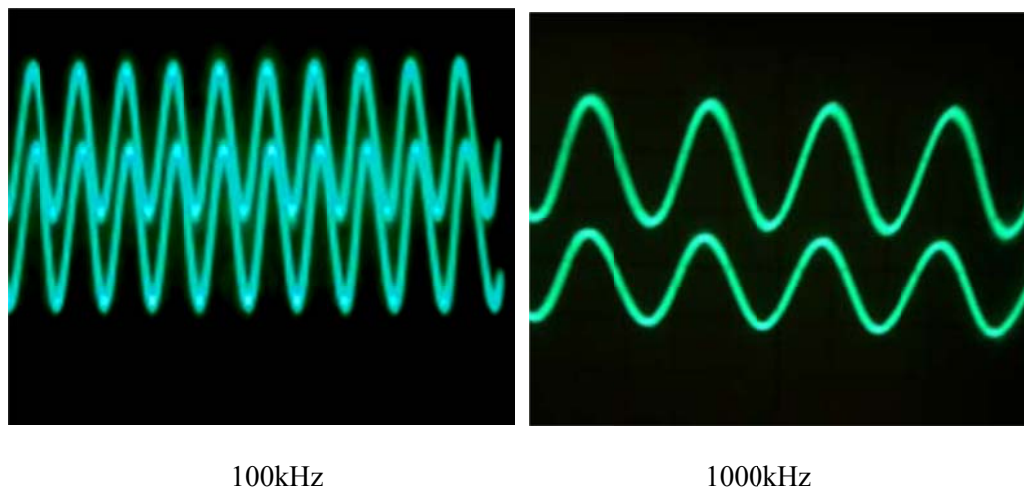
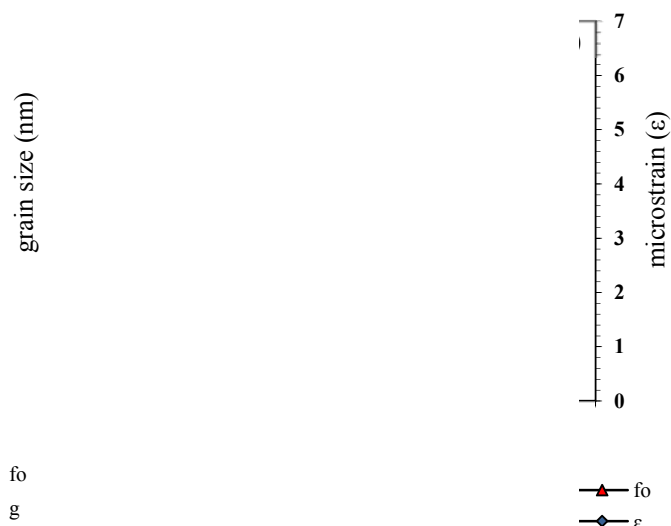


Fig. 21: The supplied frequencies (upper) and the sensing frequencies (lower) by the SnO₂ thin film at 0.4M.

The relation between resonance frequency and the structure properties which involved: grain size, micro strain and dislocation density, as a function of temperature, observed in Fig. 22. Fig. 22(a) shows that the resonance increase with temperature for 450°C then it decrease for higher increases temperature and the same behavior observed for grain size but the grain still increases for higher 450°C, but not the same relation obtained for micro strain 22(b) and dislocation density 22(c), that we can observed the same behavior for higher 450°C between structure parameters and resonance frequency.



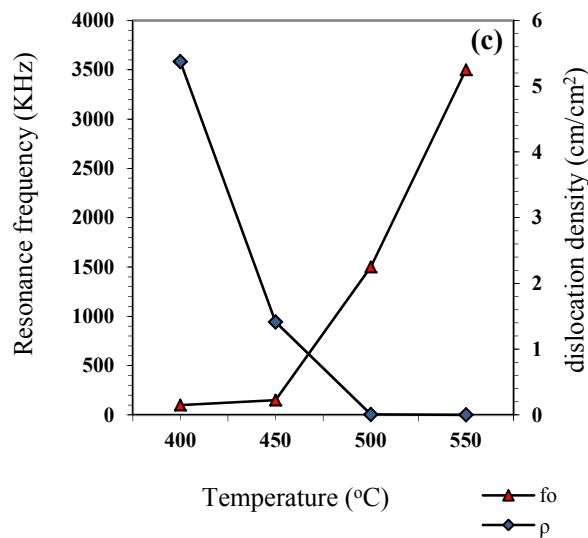
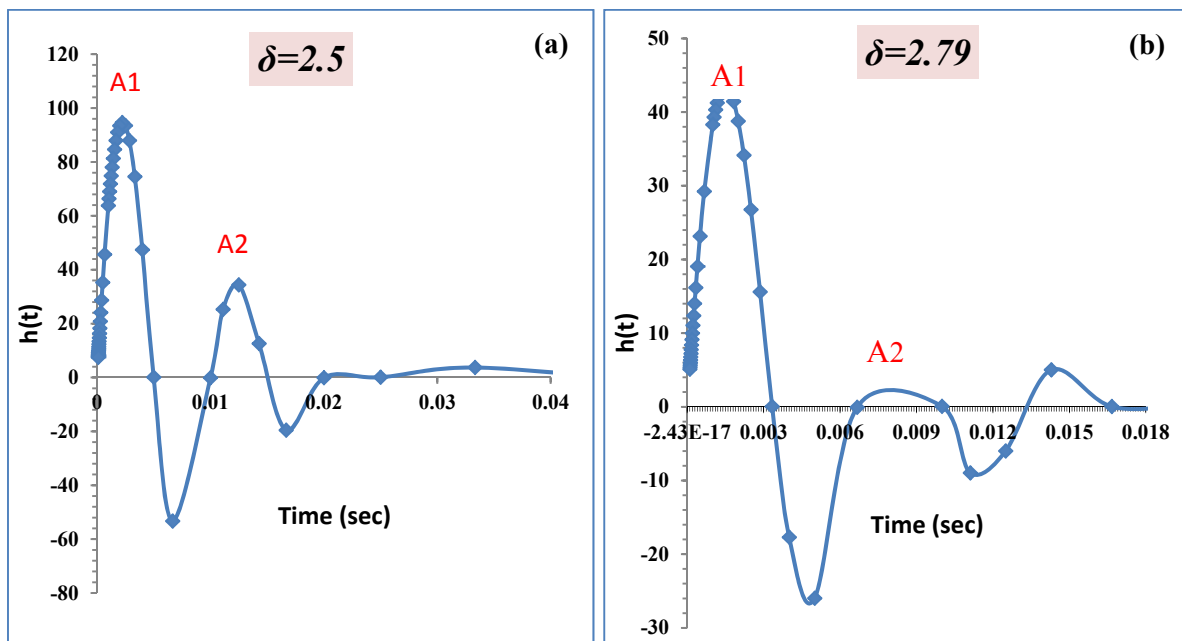


Fig. 22: The relation between resonance frequency and structure parameter as a function of substrate temperature (a) with grain size, (b) with micro strain and (c) with dislocation density.

2- Damping Coefficient (δ_D)

The damping coefficient (δ_D) can be calculated using the relation 3. Fig. 23 shown the behavior of the wave with time for different temperature, the reduce in the damping coefficient means the vibration continues for longer time because of increasing in the grain size and the arrangement of crystalline when the temperature increasing (400–550)°C.



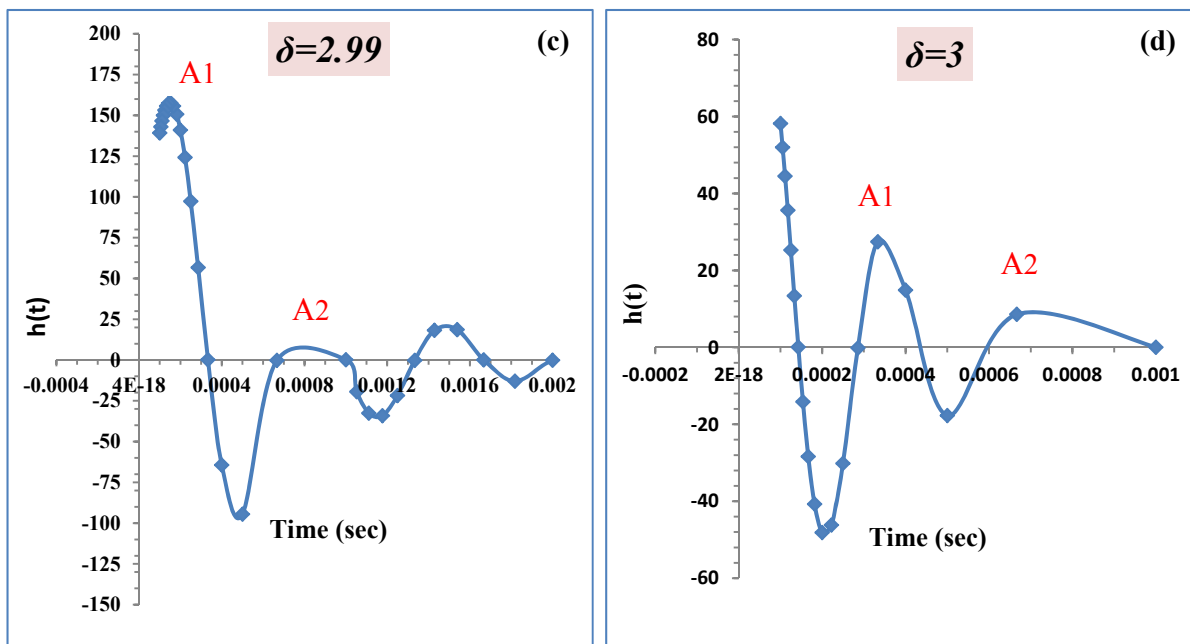
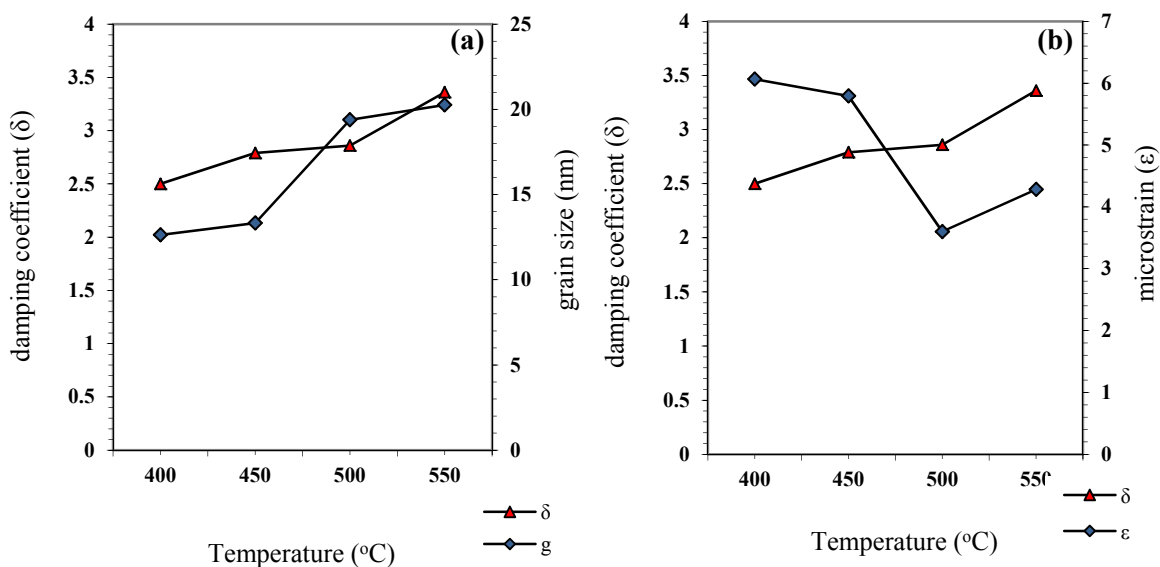


Fig. 23: The relation between the time of resonance and the damping for 0.4M at different substrate temperature (a) 400, (b) 450, (c) 500 and (d) 550.

The damping coefficient (δ_D) of the SnO₂ thin film was carried out from the graph and using the relation:

$$\delta_D = A_1 / A_2 \quad (21)$$

Fig. 24 shows clearly extrusive relation between damping and both grain size and micro strain, but there is an inverse relation between damping coefficient and dislocation density, this is meaning that the enhanced of films structure cause to increase the damping coefficient which is mean the sensitivity of the film increase.



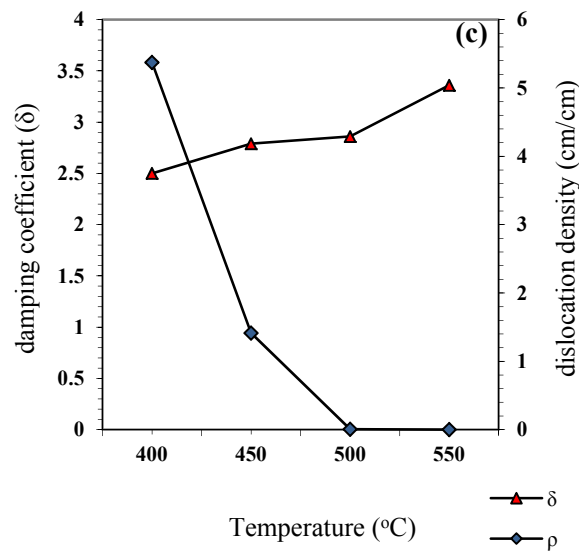


Fig. 24: the relation between damping coefficient and structure parameter as a function of substrate temperature (a) with grain size, (b) with micro strain and (c) with dislocation density.

3. Quality Factor (Q)

The relationship between the quality factor and grain size can be observed in Fig. 25(a), there is an inverse behavior between them, this may be due to increasing regular crystallization make the sensitivity of the films better and sensing high resonance frequency, which in other hand decrease the quality factor. The Fig. 25(b) shows that there is an extrusive behavior between quality factor and micro strain, where the decrease in micro strain with increase the substrate temperature means the homogeneity of the films increase and this have the same effect on the quality factor. Fig. 25(c) shows that for there is a decreasing in quality factor when the dislocation density decreased for all molarities in a different substrate temperature, and this may be because of increasing in grain size and decreasing in grain boundaries which means enhanced in the structure cause enhanced in the sensitive of the films and all of this reasons required decrease in the quality factor.

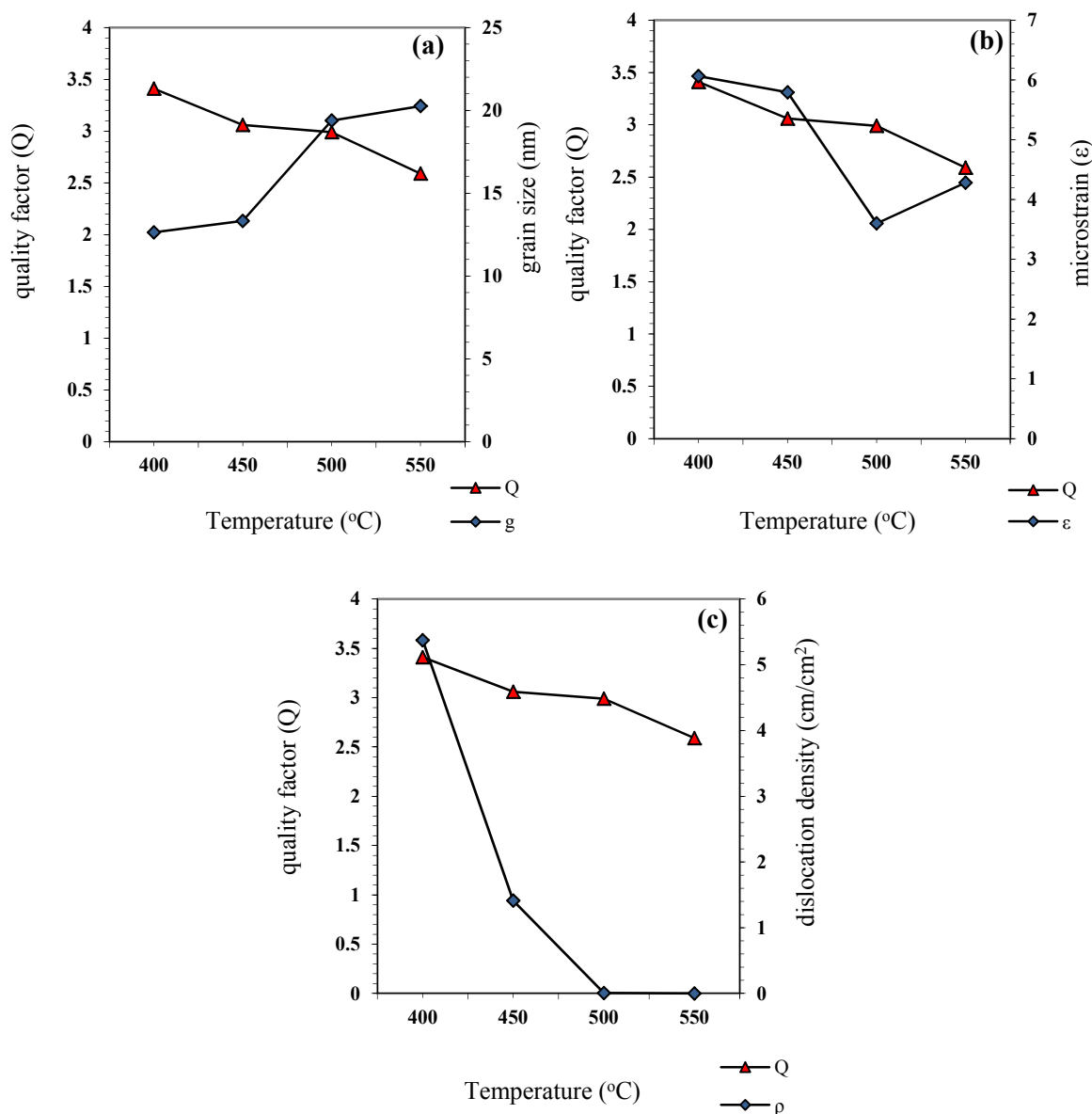


Fig. 25: the relation between quality factor and structure parameter as a function of substrate temperature (a) with grain size, (b) with micro strain and (c) with dislocation density.

Table 4: The result of piezoelectric properties.

Molarity (M)	Temperature (°C)	f ₀ (kHz)	Band width (kHz) B	Damping Coeff. (δ)	Quality factor (Q)	Surface Acoustic wave velocity (nm/sec)	Characteristic frequency f _c (kHz)
0.4	400	100	484	2.5	3.41	1538	161.7
	450	150	4595	2.79	3.06	2279	4810.5
	500	1500	2262	2.86	2.99	9877	2663.5
	550	3500	293	3.36	2.59	10422	366.13

Conclusions

The SnO₂ film prepared using Chemical Spray Pyrolysis method. SnO₂ film was found polycrystalline structure with preferred direction phase in (110) and exhibit a good structure properties which enhanced by increasing temperature. The best transmittance of SnO₂ films is (79.3%) for substrate temperature 500°C within wavelength range (300-800) nm from optical properties and this films have indirect piezoelectric phenomena where the particle was polarized when we applied an electrical current and its mechanical stress, hence the electrical force transformed into mechanical stress.

References

- [1] Puetz J., Gasparro G., Aegerter M.A., *Thin Solid Films* **442** (1–2) (2003) 40–3
- [2] Matthias B., Diebold U., *Progress in Surface Science* **79** (2–4) (2005) 47–154
- [3] Roman L Oman L.S., Valaski R., Canestraro C. D., Magalhaes E. C. S., Perrson C., Ahuja R., DA Silva Jr. E. F., Pepe I., Ferreira Da Silva A., *Applied Surface Science* **252** (15) (2006) 5361–4
- [4] Thangaraju B., *Thin Solid Films* **402** (1–2) (2002) 71–78
- [5] Nocun M., *Optical Applicata* **33** (1) (2003) 183–190
- [6] Riad A.S., Mahmoud S.A., Ibrahim A. A., *Physica B*, **296** (4) (2001) 319–25
- [7] Serin T, Serin N, Karadeniz S, Sar H, Tug LN, Pakma O., *Journal of Non- Crystalline Solids* **352** (2006) 209–215
- [8] Chatelon JP, Terrier C, Roger JA., *Science Technology*, **14** (1999) 642-647
- [9] Z. H. Zhang, B Y Sun1 and L P Shi, *Institute of Physics Publishing Journal of Physics: Conference Series* **48** (2006) 86–90
- [10] H. F. James, A. Crouch, R. Stanley, Chapter 1 (6th ed.) Cengage Learning (2007) p. 9,
- [11] T. McKinstry, Chapter 3. New York: Springer. (2008)
- [12] G. Gautschi, *Piezoelectric Sensorics: Force, Strain, Pressure, Acceleration and Acoustic Emission Sensors, Materials and Amplifiers*, Springer (2002)
- [13] G. Lippman, *Principe de la conservation de l'électricité* (in French). *Annales de chimie et de physique* **24** (1881) 145
- [14] R. R. Blanchard, *IEEE Electron Device Letters*, **20** (8) (1999)
- [15] S. O. Kasap, *Principles of Electronic Materials and Devices*, 2nd edition, McGraw Hill (2002) 557
- [16] A. A. Chernov, *Modern Crystallography III*, Chapter 1, Springer, Berlin (1984) 22
- [17] C. E. Jeffree, and N. D. Read, *Ambient and Low-temperature scanning electron microscopy*. In Hall, J. L.; Hawes, C. R. *Electron Microscopy of Plant Cells*. London: Academic Press. (1991) 313–413
- [18] A. Jasim, *Studying the Effect of Molarity on the Physical and Sensing Properties of Zinc Oxide Thin Films Prepared by Spray Pyrolysis Technique*, Al-Technological University, PhD thesis (2007)
- [19] Ali Jasim Mohammed Al-Jabiry, Marwa Abdul Muhsien Hassan, *Effect of Glucose (C₆H₁₂O₆) Addition on Piezoelectric Properties for Sensor Application*, *Sensors Applications Symposium (SAS)*, IEEE, Brescia, Italy (2012) p.1-6

- [20] J. Krautkrämer and H. Krautkrämer, *Ultrasonic Testing of Materials*, Springer–Verlag (1969)
- [21] D. Lingaraju, K. Ramji, M. Pramiladevi, Ganesh Kumar P.V.S. and B. Satya Kumar, *International Journal of Applied Engineering Research* **5** (1) (2010) 149–156
- [22] G. Nader, E. C. N. Silva and J. C. Adamowski, *J. ABCM Symposium Series in Mechatronics* **1** (2004) 271-279
- [23] S. I. Baskalov, *Signals and Circuits, Problem Solving Guide*, Mir Publishing, Moscow, (1990)
- [24] J. Lu, T.Kobayashi, R.Maeda and T.Mihara, *Quality Factor of PZT thin film transducer micro cantilevers*, Stresa, Italy (2006) 26-28
- [25] J. Lu, *SPIE Microelectronics, MEMS and Nanotechnology* (2007)
- [26] J. Lu, T. Ikehara, Y. Zhang, T. Mihara, T. Itoh and R.Maeda, *High Quality Factor Silicon Cantilever Driven by PZT Actuator for Resonant Based Mass Detection*, (2008)
- [27] H. D. Young, *University Physics*, 8th edition, Addison–Wesley Publishing Company (1991) 717-719
- [28] Z. Chen, D. Pan, B. Zhao, G. Ding, Z. Jiao, M. Wu, Chan Hung Shek, Lawrence C. M. Wu and Joseph K. L. Lai, *American Chemical Society, ACSNANO* **4** (2) (2010) 1202– 1208
- [29] Joint Committee on Powder Diffraction Standards (JCPDS), *International Center for Diffraction Data*, Swarthmore, card no. 36–1451, PA (1980)
- [30] W. Naef, K. Munz and P.G. Waser, *Histochemistry* **58** (1978) 193-201
- [31] S. A. Abass, *Determination of rystallite Size and Strain in MgO prepared by Thermal Decomposition*, University Of Saddam, Ph D. thesis (1997) 15-18
- [32] K. Kapoor, *Bull Mater. Sci.*, **27** (1) (2004) 59-67
- [33] B. Duzgun and I. Kaaraman, *Tr. J. of Physics* **22** (1998) 803- 809
- [34] B. Duzgun, *The Effect on Dislocations of Point Defects and Calculation of Strain Tensor in β -Sn Single Crystals*, Ph.D. thesis, Erzurum (1985)
- [35] K. Ojima and T. Hirokawa, *Jpn. J. Appl. Phys.* **18** (1979) p.1631
- [36] S. Mosadegh Sedghi and M. Vesali Naseh, *Proceedings of World Academy of Science, Engineering and Technology*, **37** (2070-3740) (2009)
- [37] Y. M. Poplavko, *Gallium Arsenide Application Symposium*, **132** (1996) 42-45
- [38] J. G. Van Berkum, J. G. M., A. C. Varmcuch, R. Delhen, Th. H. Dinkeijser and E. J. Hemeijer, *J. Appl. Crys.* **27** (1994) 345-357
- [39] T. Obata, K. Komeda, T. Nakao, H. Ueba and C. Tasygama, *J. Appl. Phys.* **81** (1997) 199
- [40] R. L. Mishra, Sheo. K. Mishra, S. G. Prakash, *Journal of Ovonic Research* **5**, (4) (2009) 77-85